Journal of
Materials Chemistry B

Materials for biology and medicine

Accepted Manuscript

This article can be cited before page numbers have been issued, to do this please use: X. Gu, T. Shu, W. Deng, C. shen and Y. Wu, *J. Mater. Chem. B*, 2023, DOI: 10.1039/D3TB00608E.

ROYAL SOCIETY OF CHEMISTRY

rsc.li/materials-b

View Article Online
DOI: 10.1039/D3TB00608E

X-ray activatable gold nanorod encapsulated liposome delivery system for mitochondria-targeted photodynamic therapy (PDT)

Xuefan Gu [a, d, e], Tiantian Shu [a], Wei Deng [c], Chao Shen [e] and Youshen Wu*[b]

a. College of Chemistry and Chemical Engineering, Xi'an Shiyou University, Xi'an, Shaanxi, 710065, China.

b. Department of Chemistry, School of Science, Xi'an Jiaotong University, Xi'an, Shaanxi, 710049, P. R. China

c. School of Biomedical Engineering, University of Technology Sydney, Sydney, Australia

d. ARC Centre of Excellence for Nanoscale Biophotonics, Graduate School of Biomedical Engineering, University of New South Wales Kensington 2052 NSW Australia

e. Faculty of Science and Engineering, Macquarie University, Sydney, 2109 NSW, Australia.

* Corresponding and equal senior authors

Email address: wuyoushen@mail.xjtu.edu.cn

Abstract

In this work, we developed a mitochondrially targeted nanomaterial to neoadjuvant X‐ray-triggered photodynamic therapy for rectal cancer. In our engineering, we designed biodegradable liposome incorporating a photosensitizer verteporfin to generate X-ray-induced reactive oxygen species, gold nanorods as radiation enhancers, and triphenylphosphonium acting as the mitochondrial targeting moiety. The average size of the nanocarrier was about 150 nm. Since the synergic effect between X-rays and a combination of verteporfin and gold nanorods, as well as precise site-targeted TPP-modified liposomal nanocarriers, our nanoconjugates generated sufficient cytotoxic singlet oxygen within the mitochondria upon X-ray radiation, triggering the loss of membrane potential and mitochondria-related apoptosis of cancer cells.

Keywords photodynamic therapy; liposome; gold nanorods; mitochondria-targeted; X-ray

Introduction

Photodynamic therapy (PDT), a noninvasive therapy, is undoubtedly a promising treatment modality and widely researched in clinical fields [1]. But, currently has it still not gained clinical acceptance as a first-line oncological intervention due to some limitations, such as problems in choosing the minimal light dosimetry to deep tumors,

challenges in formulating photosensitizer (PS), and difficulties in engineering precise targeted-site, etc. [2-4]. In order to deliver sufficient light to deep tumors, the X-ray-triggered PDT has emerged as a promising alternative as it is able to break through the ~1 cm tissue penetration depth limitation of activating light in traditional PDT [5-6]. Both PDT and radiotherapy are cytotoxic but via different mechanisms, providing opportunities for synergistic effects based enhanced therapeutic efficacy. In addition, the generated cytotoxic reactive oxygen species (ROS) are only within the radiotherapy field, which largely reduced possible toxicity to other healthy tissues. Essentially, the amounts of ROS are central factor for therapeutic effect of PDT and it has been reported that sufficient ROS can be produced at low doses of X-ray radiation [7]. Gold nanoparticles were demonstrated to increase X-ray-triggered ROS generation as they strongly interact with X-ray radiation owing to their radiation enhancement property in our earlier researches [8-9].

Typically, to achieve an effective and efficiency PDT treatment, the system is designed as a multifunctional nanoplatform to delivery multiple theranostic agents in a targeted manner. In this view, ideal carrier platforms are required to be biocompatible, biodegradable, tumor selective and physiochemically stable. As excellent delivery nano vehicles, liposomes with diverse formulations has been approved for clinical use now [10-11]. Of particular note is that their unique ability to encapsulate hydrophilic agents in the aqueous core and load hydrophobic agents within the lamellae depend on their concentric phospholipid vesicles consisting of single or multiple bilayered membrane structure [12]. This inherent advantage of liposomal nanoparticles definitely bestows great convenience in formulating PS and other co-loaded agents. In addition, liposomes are biodegradable and stable, which enhance system safety and PS loading efficiency [13]. Another significant chemical property of liposomes is that their surfaces are easily modified with targeting moiety or functional groups to improve expected site selectivity, thereby the efficiency of PDT (a localized therapeutic) [14].

This capability of precise targeted-site will directly determine the curative effect of PDT, because the ROS are short-lived species by nature. Singlet oxygen ($^1O_2$), one of the primary cytotoxic ROS, has a very short lifetime (half-life: 30 to 180 ns), restricting its

View Article Online
DOI: 10.1039/D3TB00608E

diffusion in biological systems to a maximum radius of ~20 nm [15]. For this reason, the targeted delivery of $^1O_2$ would be located in a subcellular organelle that sensitively responds to toxic effects of $^1O_2$. Mitochondria (~900 nm wide), power house of mammalian cells, have been preferentially selected as a target site of $^1O_2$ to improve PDT effect since they are highly susceptible to oxidative damage induced by $^1O_2$, as well as they play key roles in metabolism due to their high transmembrane potential [16]. This interior charge attracts cationic mitochondria targeting agents and even up to 500-fold accumulation of such agents in mitochondria [17]. Importantly, oncogenic changes in some mitochondria can lead to dysfunctional changes in both their ROS levels and membrane potential. As a consequence, the higher mitochondrial transmembrane potential prompt preferential accumulation and retention of cationic agents in cancer cells compared with normal cells [18]. Furthermore, the photodamaged mitochondria will instantly lose their mitochondrial membrane potential and initiate apoptosis [19]. Thus, the participation of cationic mitochondrial targeting agent in PDT can induce expeditious damage to cancer cells, improving therapeutic efficacy. Hua et al. reported cationic water-soluble Au_{25} clusters for mitochondria-targeting radioimmunotherapy [20]. The introduction of cationic units in ligands enabled the $Au_{25}(S\text{-}TPP)_{18}$ clusters to have gratifying ability to target mitochondria, which significantly enhanced their tumor killing efficacy at low dose of X-ray irradiation compared with $Au_{25}(SG)_{18}$.

In this work we designed a noble type of mitochondria-targeted liposomes that load and delivery verteporfin to the mitochondria where a low dose X-ray radiation is able to induce generation of cytotoxic $^1O_2$ from verteporfin, an efficient photosensitizer which has been clinically approved for PDT in neovascular macular degeneration [21]. Here, verteporfin was loaded inside a liposomal bilayer, referred to as lipVP. This lipVP was used to generate a sufficient amount of ROS for destabilization of the liposomal membranes under X-ray illumination. Co-encapsulation of gold nanorods (AuNRs) (10 nm) in the hydrophilic core of the liposomes enhances $^1O_2$ production by virtue of the forceful interaction between gold and X-ray radiation [9]. Scheme 1 illustrates the preparation of the liposome system and the mechanism of mitochondria-targeted PDT.

The triphenylphosphonium (TPP), as an attractive candidate for targeting moieties of conjugating mitochondria, possess the capability to target the inner mitochondrial membrane ascribed to the strong lipophilic and cationic nature of TPP [22]. These positively charged TPP-based modification of vehicles readily accumulate in the mitochondrial matrix with negative membrane potential and its multifunctional formula can be adjusted to improve its mitochondrial uptake. Currently, the most effective way to deliver cargoes specifically to mitochondria is by covalent linking a lipophilic cation such as a TPP moiety to a constructed delivery system due to their high targeting efficiency and straightforward chemical synthesis. We systematically investigated our nanocarriers *in vitro* X-ray induced PDT effect in human colorectal cancer cells (HCT116), including intracellular $^1O_2$ generation, changes in mitochondrial membrane potential ($\Delta\psi_m$), and *in vitro* cytotoxicity.

View Article Online
DOI: 10.1039/D3TB00608E

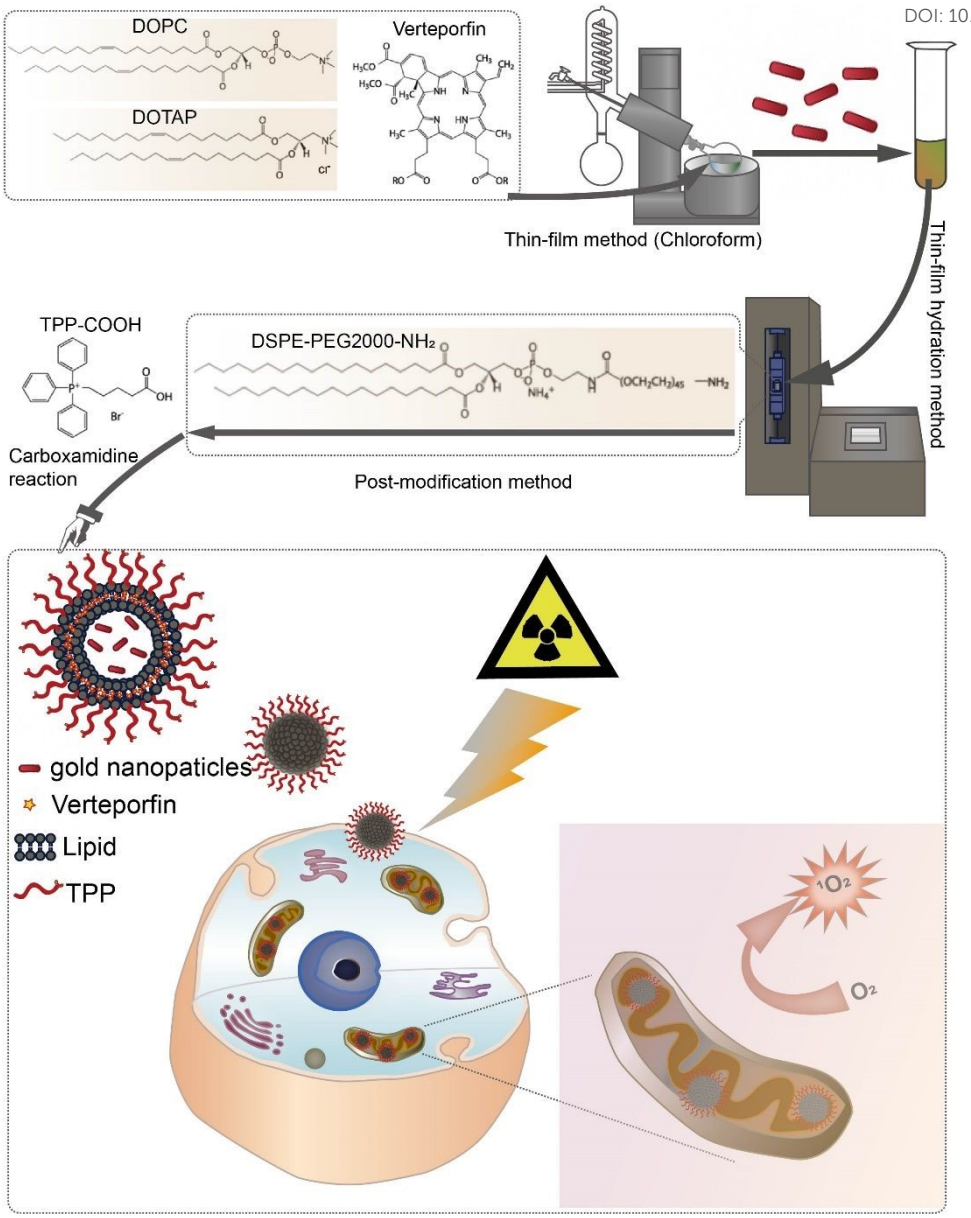

Scheme 1 The schematic illustration of (A) the liposome preparation and (B) mitochondria-targeted X-ray triggered PDT via the liposome delivery system.

Materials and methods

Materials

1,2-dioleoyl-sn-glycero-3-phosphocholine (DOPC), verteporfin, 1,2-dioleoyl-3-trimethylammonium-propane(chloride salt) (DOTAP), 10nm Gold nanorods, chloroform, dimethyl sulfoxide (DMSO), 1,2-distearoyl-sn-glycero-3-phosphoethanolamine-N-[amino(polyethylene glycol)-2000] (ammonium salt) (DSPE-PEG(2000)-NH_2), N-(3-Dimethylaminopropyl)-N'-ethylcarbodiimide hydrochloride (EDC), (4-Carboxybutyl)triphenylphosphonium bromide (TPP-

COOH), N-Hydroxysuccinimide (NHS), 2-(N-Morpholino) ethanesulfonic acid (MES), Methanol, and McCoy's 5A Medium were purchased from Sigma-Aldrich Pty Ltd. Singlet Oxygen Sensor Green (SOSG), live cell imaging solution, Fetal Bovine Serum (FBS) and Dulbecco's Phosphate-Buffered Saline (DPBS) were purchased from Thermo Fisher Scientific Inc. JC-1-mitochondrial membrane potential assay kit was purchased from Abcam Corporation. CellTiter 96® AQueous one solution cell proliferation assay were purchased from Promega Corporation.

Methods

Preparation of pure liposomes and liposomes encapsulating gold nanorods and VP. Liposome-based nanocarriers in this study were prepared via a thin-film hydration method [8]. Briefly, 25μL of DOPC (100mM) was mixed with 25μL of DOTAP (100mM) dissolved in chloroform and subsequently added of 4μL VP solution (3mM, dissolved in DMSO). For the synthesis of pure liposomes and liposomes incorporating gold nanorods alone, VP were omitted in the mixture solution. The system solvent was then evaporated using a rotary evaporator (Rotavapor® R-300, BÜCHI) for 10 min at 70 ^{o}C. The thin lipid film was formed around the inner wall of the flask, followed by hydration with PBS buffer (pH 7.4) (in the case of pure liposomes and liposomes loaded with VP only) or gold nanorods suspension (in the case of liposomes loaded with VP and gold nanorods) with vigorous stirring for 30 min until the suspension was homogenized (Vortexer, Heathrow Scientific). It is worth emphasizing that the liposomes including AuNRs were obtained after centrifugation and free AuNRs can be separated by centrifugation at a lower speed due to their relative high density compared with liposomes. The hydrated lipid suspension was kept away from light at room temperature for 3 hr to allow the maximal swelling of liposomes. The suspension was then extruded eleven times through a 200 nm polycarbonate membrane using an automated extrusion equipment (NanoSizerTM AUTO, T&T Scientific Corporation, USA). The resultant suspension was stored at 4°C.

View Article Online
DOI: 10.1039/D3TB00608E

Characterisation of liposomes. We prepared several types of liposome samples including liposomes incorporating VP and gold nanorod (Lipo-VP-AuNRs), liposomes containing VP (Lipo-VP) only and pure liposomes. Size distribution and ζ potentials of these liposomes were determined under a Zetasizer Nano-ZS from Malvern Panalytical Co. The extinction spectra of pure gold nanorods (AuNRs) colloidal solution and preformed liposome samples were measured using a spectrophotometer (Cary 5000 UV-Vis-NIR, Agilent Technologies). The morphology of liposomes was observed via Transmission Electron Microscopy (TEM). As for TEM imaging, the liposome samples were prepared by locating a drop of suspension onto a copper grid and air dried, as well as subsequent negative staining for contrast enhancement. The air-dried samples were then imaged by a PHILIPS CM 10 system at an accelerating voltage of 100 KV. Images were captured with iTEM software and an Olympus Megaview G10 camera. The loading amount of gold nanorods in liposomes was calculated based on Thermogravimetric Experiment (TGA 2, METTLER TOLEDO).

Liposome surface modification with TPP-COOH. In order to inhibit PEG-lipid degradation and prolong the circulation time, PEGylated liposomes were prepared via post-insertion of DSPE-PEG(2000)-NH_2 micelles into prepared liposomes [23]. Subsequently, TPP-modified liposomes were further prepared based on EDC-NHS coupling method with slight modifications. This method not only had high synthetic yield, but also avoided the low surface loading rate caused by the hydrophobicity of TTP, compared with adding the TPP coating from the beginning. In detail, 500μL of preformed liposomes and 50μL of DSPE-PEG(2000)-NH_2 (0.01M in distilled water) co-incubated at 60°C for 1h, followed by centrifugation 3 times (11000 rpm, 10min) with Amicon Ultra 0.5mL centrifugal filters (100 kDa) in order to remove the free molecules. After that a mixture of EDC and NHS (molar ratio, 1:1) was added, following dissolving of TPP-COOH (10 mg) in 1 ml MES buffer (pH=6). The solution was kept stirring away from light at room temperature for 30 min and subsequent addition of aforementioned PEGylated liposome suspension (200 μL) into the activated

TPP solution (pH 7.0-7.4). The system was gently vibrated by orbital shaker for 4h at room temperature and then washed with PBS buffer three times (11000rpm, 10min each time) with Amicon Ultra centrifugal filters (100 kDa). The resultant liposome conjugate suspension was kept at 4°C for future use.

Evaluation of $^1O_2$ generation from the liposome samples under X-ray radiation. $^1O_2$ generation was measured by employing SOSG probe and the irradiation of samples was carried out by using 320 kV cabinet X-Ray Irradiator (X-RAD 320, Precision X-Ray, Inc.). The fluorescence signal of SOSG (excitation/emission wavelength: 488/525 nm) was recorded before and after X-ray radiation via a spectrofluorometer (FluoroMax-4 HORIBA Scientific Co.).

Cell culture and X-ray radiation on cells. Normal human colon epithelial cells (CCD841 CoN) and human colon adenocarcinoma (HCT116 cells) were purchased from the American Type Culture Collection. CCD841 CoN cells were cultured in EMEM and HCT116 cells were cultured in McCoy's 5 A (modified) medium. All culture media in this work were supplemented with 10% FBS and 1% antibiotic-antimycotic. The flasks were incubated at 37°C in the existence of 5% CO_2 humidified air. The cells were cultured at advisable dilutions into 96-well plates for *in vitro* cell viability assays or glass-bottom petri dishes for cell imaging analysis. As for X-ray radiation investigation, the cells were radiated via the same X-ray irradiator as mentioned above in the $^1O_2$ production evaluation.

Analysis of cellular uptake of the liposomes. HCT116 cells (10^4 cells/mL) were cultured with prepared liposome suspension in incubator for flow cytometry measurements. The cells were then washed three times with Dulbecco's phosphate buffered saline, trypsinized, centrifuged at 3000 rpm for 3 min, and resuspended in DPBS. For assessment of the cellular uptake activity of the liposomes, the cells were monitored by using a flow cytometer (LSRFortessa™ X-20 cell analyser, BD Biosciences) equipped with a violet laser. FlowJo software was used for further calculation of FCM data.

Intracellular $^1O_2$ detection. HCT116 cells were seeded in glass-bottom petri dishes at a concentration of 1×10^5 cells/mL and were then treated with different

View Article Online
DOI: 10.1039/D3TB00608E

liposome samples (250 μM) in culture media for 3 h at incubator, as well as subsequent addition of SOSG solution (50μM) for further 1 hr incubation). After that the cells were irradiated with X-rays at different doses in fresh media, followed by using FV3000 confocal laser scanning microscope to achieve visual image of SOSG fluorescence signal. A laser at 488 nm was employed for SOSG excitation. Furthermore, the intracellular $^1O_2$ level generated under different experimental conditions were accurately assessed based on quantitative analysis of SOSG signal via ImageJ software.

Evaluation on mitochondrial membrane potential ($\Delta\psi_m$). HCT116 cell were seeded and treated with liposome-TPP conjugates or non-conjugated liposomes in the cell media for 4 hr, followed by X-ray radiation at 4Gy. After further 24 hr incubation, cells were stained with 5 μM cationic dye tetraethylbenzimidazolylcarbocyanine iodide (JC-1) probe at 37°C for 15 min for fluorescence imaging. The ratio of JC-1 probe aggregates (red signal) to monomers fluorescence (green signal) are often employed to indicate alterations in Δψm, as aggregated JC-1 dye in normal mitochondrial membrane emitting red fluorescence, contrarily JC-1 monomers in the damaged mitochondria emitting green fluorescence. The $\Delta\psi_m$ analysis was conducted by comparing JC-1 fluorescence signal at 590±17 nm (red aggregates) with that at 530±15 nm (green monomers), and using ImageJ software to quantitively analyse the ratio of red-to-green channel intensities.

***In vitro* cytotoxicity after X-ray triggered PDT.** The four groups of cells (1×10^4 /mL) for cellular viability assay were planted onto 96-well plates and incubated for 48 hr at 37°C, including untreated control cells, liposomes treated cells cultured, X-ray treated cells, as well as cells treated with X-ray induced PDT. At 24 hr corresponding post treatment, cellular cytotoxicity was evaluated by employing the Cell Viability Assay Kit, MTS (Promega Corporation, USA) according to its protocol. The further quantitative analysis of cell viability by using a plate reader (SpectraMax MiniMax 300 Imaging Cytometer, Molecular

Devices) and calculated as a percentage of the absorbance of the control cells that was set to 100%.

X-ray radiation in vitro deep tissue imaging.

To investigate the feasibility of X-ray-triggered persistent luminescence for deep-seated tissue-penetration depth, *in vitro* cellular viability of cells treated with X-ray induced PDT in a 96-well plate covered with pork tissues at different thicknesses (0, 2, 4 cm) was assessed using aforementioned MTS assay and a plate reader.

Statistical analysis. All quantitative data are shown as mean ± SD, n ≥ 3. Statistical analysis was carried out using GraphPad Prism t test calculator and **p*< 0.05, ***p*< 0.01, ****p*< 0.001, *****p*< 0.0001.

Results and discussion

Characterization of liposomes loaded with VP and gold nanorods

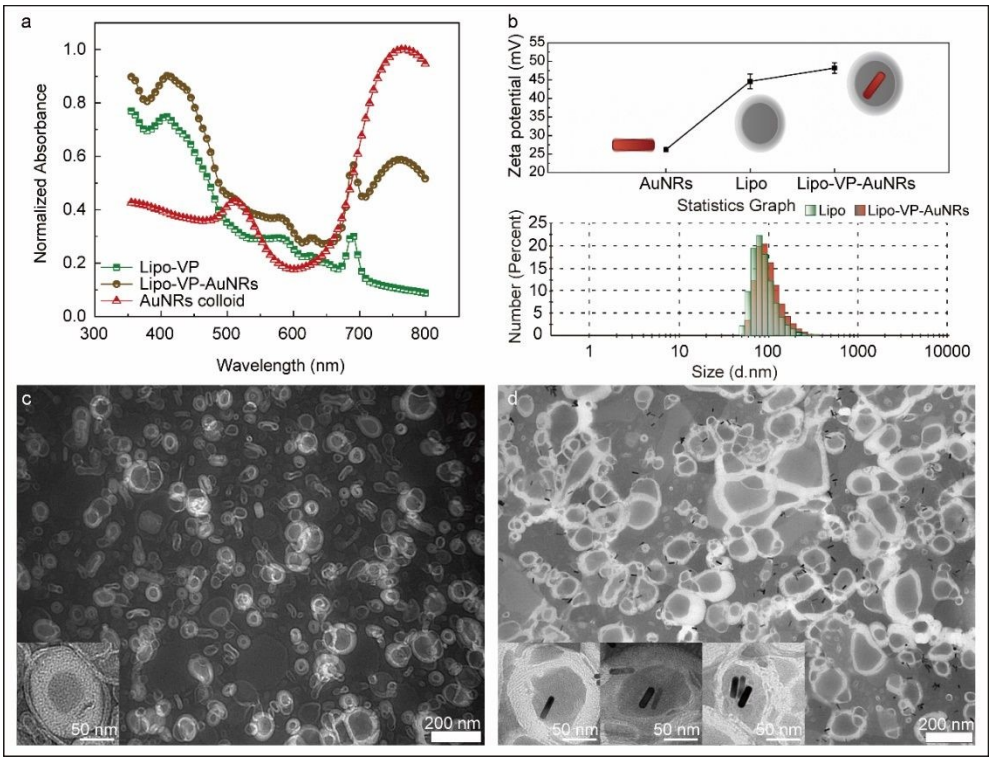

Figure 1 Characterisation of different liposome samples and AuNRs. **(a)** Absorption spectra of Lipo-VP, Lipo-VP-AuNRs and pure AuNRs colloidal solution. **(b)** ζ potential and size distribution determined by dynamic light scattering. TEM images of **(c)** pure liposomes and **(d)** liposomes encapsulating AuNRs;

inset is a TEM image of the same sample under high magnification. AuNRs encapsulated in liposomes were clearly observed under TEM with high magnification.

Fig.1a displays the extinction spectra of Lipo-VP, Lipo-VP-AuNRs and AuNRs colloidal solution, where typical absorption peaks from both VP and AuNRs were observed. The two characteristic absorption peaks of VP around 410 nm and 690 nm were obviously observed in both Lipo-VP and Lipo-VP-AuNRs, indicating cargo of VP. Compared with Lipo-VP, Lipo-VP-AuNRs has a further absorption peaks around 780 nm, which is consistent with that in AuNRs colloidal solution. The three distinct absorption peaks of Lipo-VP-AuNRs confirm the co-encapsulation of VP and AuNRs in the liposomal membranes. In addition, the loading amount of gold nanorods in liposomes was 1.1% according to Thermogravimetric Experiment.

Furthermore, the TEM image shows the morphology of liposomes loaded with AuNRs, illustrating that the 10 nm AuNRs were incorporated in the hydrophilic core (Fig. 1d). Recently, the location of gold nanoparticles in nanoscopic carriers with amphiphilic structure attracts more attention and various engineering of diverse gold nanoparticles through encapsulation or coating into vehicles are reported [24-26]. Interestingly, the precise gold nanoparticles localization in the hydrophilic or hydrophobic liposome cavity could further affect the physical and chemical properties, as well as physiological functions of liposome conjugates [27]. Generally, the structures of hybrid liposome-gold are classified into three categories, including gold coated on liposome surface, gold embedded in hydrophobic bilayer and gold encapsulated within hydrophilic core [28-34].

In most of gold-coated liposomes incorporating other optical or bioactive encapsulants studies, several groups have observed gold increased the apoptosis of PDT/PTT-treated tumor cells, especially liposomes coated with AuNRs possess both efficient PDT and PTT effect using clinically acceptable irradiation power [28-29]. Apart from this surface coating liposome–gold assemblies, the fabrication of other two kind of gold interior have more active sites on liposomal surface to connect with functional groups, such as smart responsive ligand and targeting moiety [33-34]. Thus, we designed the interior payload in this liposome formulation and fully used double phospholipid layer

structure of liposome. AuNPs were located in the hydrophilic core and hydrophobic VP molecules were entrapped in the hydrophobic bilayer. The electric charge and bioactive/chemactive group of bare liposomal surface can be easily regulated by changing the species and molar ratio of lipid candidates. We optimized our liposome formulation here based on our previous work [8], and ζ potential of pure liposome was 44.6mV, very close to Lipo-VP-AuNRs (47.2mV) (Fig. 1b). Their nearly equal ζ potential values indicated that AuNRs were encapsulated in the liposome. And the high ζ potential value not only revealed the physical and chemical stability of the liposome–gold colloidal solution, but also offer a charge-rich microenvironment for sequent preparing PEGylated liposomes via post-insertion method.

In addition, our engineering of Lipo-VP-AuNRs also exhibited good monodispersity, as the hydrated diameter of pure liposome and Lipo-VP-AuNRs was 146.9nm (PDI: 0.160) and 143.5nm (PDI: 0.222), respectively (Fig. 1b), confirming the AuNRs in this design have no effect on vehicles size. This result is consistent with the observation of TEM images (Fig. 1c, 1d). Importantly, inset of TEM image under high magnification also illustrated that the bilayer thickness (~8nm) of pure liposome nearly the same with Lipo-VP-AuNRs. In contrast with hybrid lipid nanocarrier containing bilayer-embedded hydrophobic gold nanoparticles, our architecture in this work have advantages in no effect on bilayer thickness, more encapsulation efficiency, more anisotropic gold candidate with diverse size. Furthermore, the prepared Lipo-VP-AuNRs with homogenized size below 200nm and sable bilayer micromorphology are beneficial to normal metabolism and reducing encapsulants leakage [35-36].

View Article Online
DOI: 10.1039/D3TB00608E

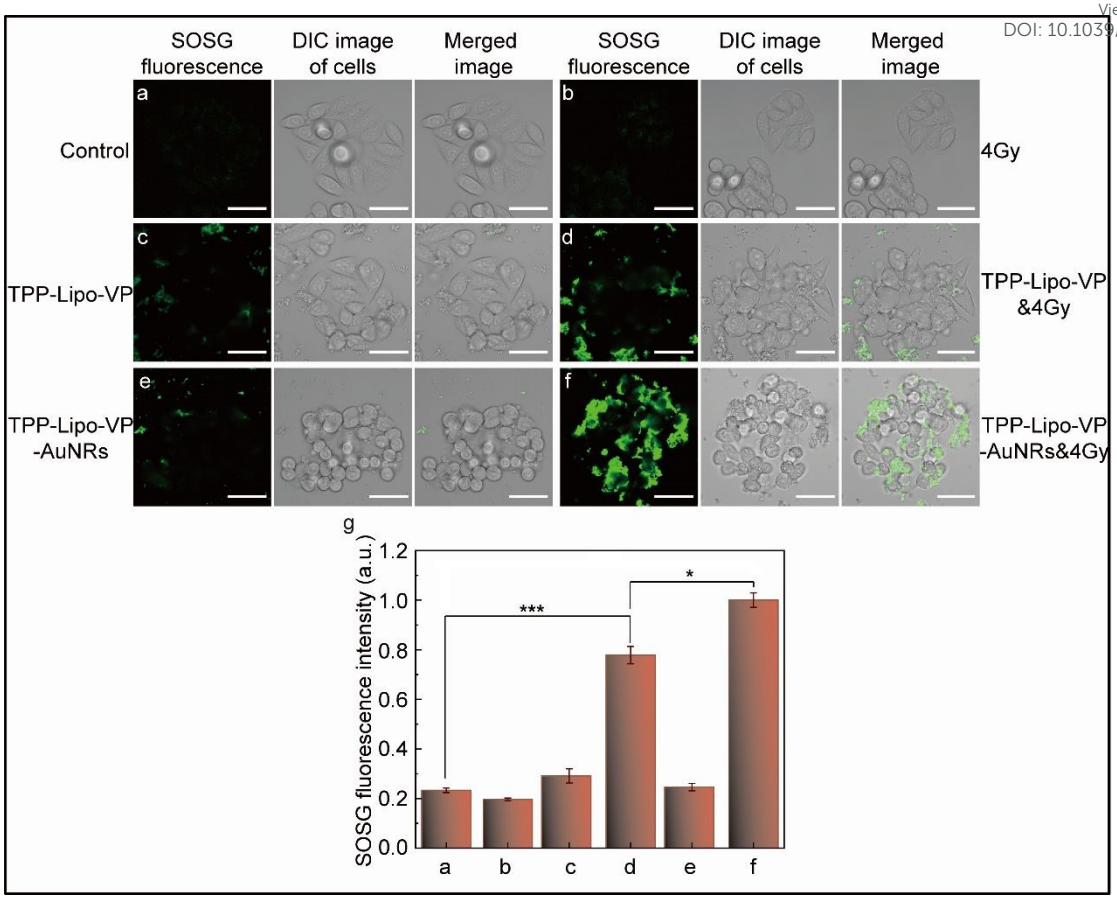

Figure 2 Intracellular $^1O_2$ generation from liposomes with and without X-ray radiation. **(a-f)** Representative confocal laser scanning microscopy images of SOSG in **(a)** HCT116 cells without any treatment, **(b)** HCT116 cells after 4Gy X-ray irradiation, **(c)** HCT116 cells treated with TPP-Lipo-VP (250 μM) for 2 hr, **(d)** HCT116 cells treated with TPP-Lipo-VP (250 μM) for 2 hr and 4Gy X-ray irradiation, **(e)** HCT116 cells treated with Lipo-VP-AuNRs (250 μM) for 2 hr and **(f)** HCT116 cells treated with Lipo-VP-AuNRs (250 μM) for 2 hr and 4Gy X-ray irradiation. Scale bar is 30μm. (g) Quantitative calculation of $^1O_2$ generation in HCT116 cells at different treatment conditions**.**

Evaluation of Intracellular $^1O_2$ Generation

The generation of cytotoxic $^1O_2$ is a key factor responsible for X-ray-induced PDT effect, leading to the disruption of the liposome structure. $^1O_2$ production was confirmed by employing singlet oxygen sensor green (SOSG) and measuring the enhancement of fluorescence intensity at 525 nm for 488 nm excitation [8]. We evaluated the $^1O_2$ generation in solution and checked the SOSG fluorescence intensity of prepared samples at 525nm wavelength under different X-ray dosage as shown in

Supplementary Figure 1a. Among the tested liposomes, the maximum enhancement of $^1O_2$ production was achieved in the presence of AuNRs, which is consistent with our previous work [8]. Subsequently, we compared intracellular $^1O_2$ generation from our prepared liposome samples under different treatment conditions (liposome samples ± 4 Gy X-ray radiation) as shown in Figure 2.

An obvious higher $^1O_2$ generation was observed in the cells treated with X-ray induced liposome samples loaded with VP (Fig. 2d and f) compared with control (Fig. 2a), in contrast with nearly no difference between untreated control cells and cells only induced under 4Gy X-ray radiation (Fig. 2b). This phenomenon indicates that the dosage of 4 Gy is nontoxic for the cell treatment. An approximate amount of $^1O_2$ was also found in the cell groups respectively treated with TPP-Lipo-VP and TPP-Lipo-VP-AuNRs alone (Fig. 2c and e), confirming the safety of aforementioned liposome samples. These data revealed that cells treated with liposome incorporating VP combined with X-ray radiation can be triggered to produce apparent $^1O_2$. Additionally, the SOSG intensity of TPP-Lipo-VP-AuNRs incubated cells are demonstrably higher than the cells treated by TPP-Lipo-VP and ascribed to the following mechanism. As an outstanding radiosensitizers, gold nanoparticles have capability to amplify the radiation doses in tumor tissue [37]. Thus, the VP molecules in the co-existence of gold nanoparticles have capability to interact more strongly with ionising radiation than the VP alone, causing enhanced $^1O_2$ production. The significantly highest signal of SOSG fluorescence observed in Fig. 2 f demonstrates the hydrophobic VP co-existent with hydrophilic AuNRs encapsulated in our liposomal nanomaterials can be activated from X-ray triggering even at low dosage, resulting in sufficient $^1O_2$ for PDT.

It is also informed that vehicles with TPP moiety have a distinguished mitochondrial selectivity and TPP-conjugated nanomaterials are widely used to locate to the mitochondria of several types of cancer [38-39]. Such mitochondrial targeted-site is beneficial to improve $^1O_2$ utilization, because mitochondria are highly susceptible to oxidative damage induced by $^1O_2$, causing apoptosis of cancer cells [40-41]. Since the generated $^1O_2$ has a diffusion radius (~20 nm) and short lifetime (~40 ns), engineering TPP-Lipo-VP with capability of preferentially targeting mitochondrial (~900 nm wide)

View Article Online
DOI: 10.1039/D3TB00608E

can maximally enhance PDT efficiency [42].

To further assess the role of precise targeted-site on improve PDT therapeutic effect, we studied the difference of cellular uptake between Lipo-VP treated triggerable cells and TPP-Lipo-VP treated triggerable cells as shown in Supplementary Figure 1c. We compared the cellular uptake of Lipo-VP and TPP-Lipo-VP in the HCT116 cells by incubating the cells with Lipo-VP or TPP-Lipo-VP for 1 h, 2 h and 4 h, respectively. The pseudo green color from VP in TPP-Lipo-VP treated cells was obviously noticed after 2 h incubation time, nearly comparable to that observed in Lipo-VP treated cells after 4 h incubation time. These results suggest that TPP-modified liposomes can be rapidly absorbed and aggregated in tumors compared to unmodified ones. The chemical structure of TPP-Lipo-VP was confirmed with ^{1}H NMR spectrum (Supplementary Figure 1b) and the characteristic peaks at 7.78 ppm in the spectrum was attributed the proton of benzene from TPP in accordance with that reported in the literature [43]. These results implied that the TPP modified liposomal conjugate was synthesized successfully. In addition, the statistical amount of pseudo green color in TPP-Lipo-VP treated cells were nearly equivalent after 2 h and 4 h treatment time, respectively, indicating cellular uptake of TPP-Lipo-VP reaches saturation after 2 h incubation. Thus, we chose 2 h incubated TPP-modified liposomes as the therapeutic nanocarriers for further cellular experiments.

View Article Online
DOI: 10.1039/D3TB00608E

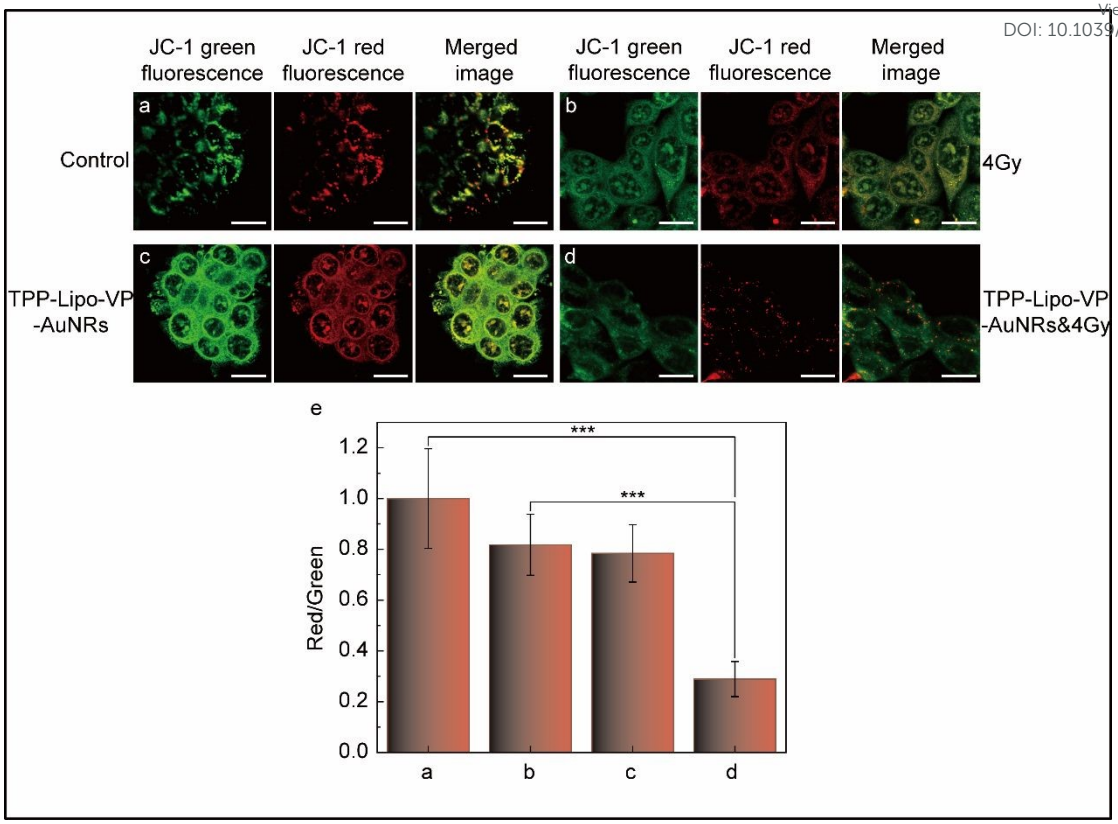

Figure 3 Changes in JC-1 fluorescence signal ($\Delta\psi_m$) in HCT116 cells under different treatment conditions: **(a)** the cells without any treatment, **(b)** the cells treated with 4Gy X-ray radiation, **(c)** the cells treated with Lipo-VP-AuNRs (250 μM) and **(d)** the cells treated with Lipo-VP-AuNRs (250 μM) and 4Gy X-ray radiation. Scale bar is 20 μm. The low membrane potential caused the monodispersed release of JC-1 to the cytosol, as shown by the strong green fluorescent signal, and high-membrane potential resulted in the JC-1 aggregation in the membrane, as shown by the strong red fluorescent signal. **(e)** Red-to-green channel ratio dictates the rate of membrane potential decay and cells dead.

Assessment of Mitochondria Membrane Potential ($\Delta\Psi_m$)

Aforementioned data confirm that triggered intracellular $^1O_2$ generation is enhanced by the synergic effect between X-rays and a combination of VP and AuNRs, as well as TPP-modified liposomal nanocarriers further improve $^1O_2$ utilization in our engineering. TPP moiety, representative lipophilic mitochondria-targeting cations, facilitate the TPP-based vehicles attaching to the negative mitochondrial inner membrane for chemotherapeutic and diagnostic applications [22]. Mitochondria is thought to play a crucial role in apoptosis and $\Delta\psi_m$ is reported to contribute to cell death by disruption of normal mitochondrial function [44]. To deepen the exploration of the enhanced

radiosensitization mechanism of TPP-conjugated delivery targeting mitochondria, $\Delta\psi_m$ was monitored to evaluate the mitochondrial function after liposome administration with X-ray via JC-1 staining (a mitochondrial membrane potential dye) and confocal microscopy. The ratio of JC-1 probe aggregates (red signal) to monomers fluorescence (green signal) are often employed to indicate alterations in $\Delta\psi_m$, as aggregated JC-1 dye in normal mitochondrial membrane emitting red fluorescence, contrarily JC-1 monomers in the damaged mitochondria emitting green fluorescence [45]. As shown in Fig.3a, b and c, the JC-1 signal was slightly changed in the cells treated with TPP-Lipo-VP-AuNRs alone or induced by 4 Gy radiation alone, compared with the untreated group. This manifest acceptable toxicity of TPP-Lipo-VP-AuNRs in HCT116 cells and tolerable toxicity of 4 Gy radiation, which was consistent with our following in vitro cytotoxicity experiment (Fig.4a, b and d). However, the samples treated with TPP-Lipo-VP-AuNRs exposed to 4 Gy X-ray radiation presented a sharply decreasing red/green ratio, representing the maximum mitochondrial depolarization and $\Delta\psi_m$ damage as consequence of cytotoxic $^1O_2$ produced by X-ray induced PDT effect. The result not only supports the previous data for greatest intracellular $^1O_2$ production from cells incubated with TPP-Lipo-VP-AuNRs at 4 Gy X-ray (Fig.2f), but also confirm that mitochondria are exactly vulnerable to oxidative damage caused by $^1O_2$.

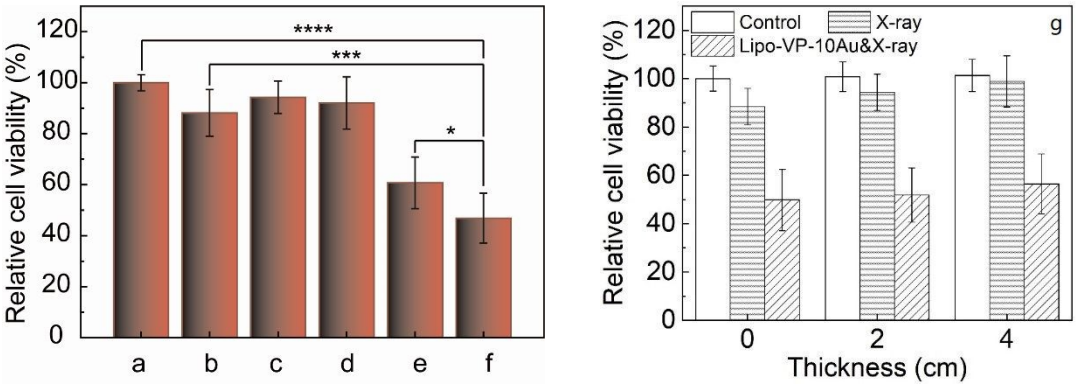

Figure 4(**a-f)** *In vitro* cytotoxicity in HCT116 cells after different treatments**. (a)** the cells without any treatment, **(b)** the cells treated with 4Gy X-ray radiation, **(c)** and **(d)** the cells treated with TPP-Lipo-VP and TPP-Lipo-VP-AuNRs (250 μM), respectively, **(e)** and **(f)** the cells treated with 4Gy X-ray radiation combined with TPP-Lipo-VP or TPP-Lipo-VP-AuNRs (250 μM). **(g)** Impact of tissue depth on X-ray induced PDT efficiency.

View Article Online
DOI: 10.1039/D3TB00608E

Assessment of Cell Viability after X-PDT

To evaluate cell viability all aforementioned the treatments, cytotoxic effects were tested by MTS assay. We first assessed the toxicity of liposome-formulated VP designed in this work, including TPP-Lipo-VP (Fig. 4c) and TPP-Lipo-VP-AuNRs (Fig. 4d). Compared with the control group (Fig. 4a), both TPP-Lipo-VP and TPP-Lipo-VP-AuNRs caused minimal changes to HCT116 cell viability, nearly similar with the HCT116 cell survival exposed to 4 Gy radiation alone. The results confirmed that the prepared nanomaterials and the selected dosage are reliable to improve PDT efficiency. However, when these two nanomaterials treated cells combined with X-ray radiation (4 Gy), high induced cytotoxicity in HCT116 cell was observed, particularly the incubated TPP-Lipo-VP-AuNRs cells (46.9%). This remarkable enhanced cytotoxicity effect is as the consequence of sufficient $^1O_2$ produced by activated VP at 4 Gy radiation and augmented by the X-ray-sensitive AuNRs, supporting the efficient intracellular $^1O_2$ generation (Fig. 2f) and significant decrease of $\Delta\psi_m$ (Fig. 3d) mentioned above. It can be seen that the targeting effect of TPP-modified liposomes on mitochondria can effectively enhance the killing of cells by irradiation, and through this targeting synergy, the effect of irradiation therapy can be effectively improved.

X-ray-triggered theranostics is known to penetrate deep inside the body [46]. Given this, we further investigated *in vitro* X-ray induced PDT to cause efficient HCT16 cells death using pork as a model tissue. Herein, we sought to evaluate the effect of X-ray radiation penetration depth on cytotoxicity in TPP-Lipo-VP-AuNRs-treated HCT16 cells stacked with a thick piece of pork meat (2 and 4 cm), as shown in figure 4g. The cell viability of HCT116 tumor cells stacked with pork meat (2 and 4 cm) under X-ray radiation are approximative to that of control group. However, the cells treated with TPP-Lipo-VP-AuNRs and stacked with pork meat (2 and 4 cm) at 4 Gy exhibited obvious cytotoxicity, cell survival dropped to 51.8% and 56.4%, respectively. These results were comparable to those samples without pork interference only under X-ray irradiation, indicating a relatively trivial impact of tissue depth on treatment efficacy.

Conclusions

We have constructed a noble type of mitochondrially-targeted liposomal delivery system to enhanced X-ray PDT effect in deep tissue. The TPP modified multifunctional liposomes with amphiphilic structure encapsulated hydrophilic AuNRs in the aqueous core and incorporated hydrophobic VP within the bilayer. Since the mitochondria-targeting capacity of TPP and strong interaction between gold and X-ray radiation, sufficient enhanced $^1O_2$ generation and effective utilization were achieved in HCT116 cells at a low dose X-ray radiation.

Funding

This work was financially supported by the Funding (GNT1181889) from the Australia National Health and Medical Research Council, fellowship award (2019/CDF1013) from New South Wales Cancer Institute, Australia.

Notes and references

[1] K. Deng, C. X. Li, S. S. Huang, B. G. Xing, D.Y. Jin, Q. G, Zeng, Z. Y. Hou and J. Lin, *Small*, 2017, **13**, 1702299.

[2] A. Master, M. Livingston and A. S. Gupta, *J. Control. Release*, 2013, **168**, 88-102.

[3] Z. Kautzka, S. Clement, E. M. Goldys and W. Deng, *Int. J. Nanomed.*, 2017, **12**, 969-977.

[4] S. S. Lucky, K. C. Soo and Y. Zhang, *Chem. Rev.*, 2015, **115**, 1990-2042.

[5] L. Larue, A. Ben Mihoub, Z. Youssef, L. Colombeau, S. Acherar, J. C. André, P. Arnoux, F. Baros, M. Vermandel and C. Frochot, *Photoch. Photobio. Sci.*, 2018, **17**, 1612-1650.

[6] G. D Wang, H. T. Nguyen, H. M. Chen, P. B. Cox, L. C. Wang, K. Nagata, Z. L. Hao, A. Wang, Z. B. Li and J. Xie, *Theranostics*, 2016, **6**, 2295-2305.

[7] X. F. Chen, J. B. Song, X. Y. Chen and H. H. Yang, *Chem. Soc. Rev.*, 2019, **48**, 3073-3101.

[8] W. Deng, W. J. Chen, S. Clement, A. Guller, Z. J. Zhao, A. Engel and E. M. Goldys, *Nat. Commun.*, 2018, **9**, 2713.

[9] W. Deng, K. J. McKelvey, A. Guller, A. Fayzullin, J. M. Campbell, S. Clement, A. Habibalahi, Z. Wargocka, L. E. Liang, C. Shen, V. M. Howell, A. F. Engel, E. M. Goldys, *ACS Cent. Sci.*, 2020, **6**, 715-726.

[10] Z. Al-Ahmady and K. Kostarelos, *Chem. Rev.*, 2016, **116**, 3883-3918.

View Article Online
DOI: 10.1039/D3TB00608E

[11] Y. C. Fan and Q. Zhang, *Asian J. Pharm. Sci*., 2013, **8**, 81-87.

[12] Q. P. Li, W. Li, H. X. Di, L. H. Luo, C. Q. Zhu, J. Yang, X. Y. Yin, H. Yin, J. Q. Gao, Y.Z. Du and J. You, *J. Control. Release*., 2018, **277**, 114-125.

[13] T. Lajunen, L.-S. Kontturi, L. Viitala, M. Manna, O. Cramariuc, T. Róg, A. Bunker, T. Laaksonen, T. Viitala, L. Murtomäki and Arto Urtti, *Mol. Pharmacol*., 2016, **13**, 2095-2107.

[14] F. Y. Zhou, B.Feng, T. T. Wang, D. G. Wang, Z. R. Cui, S. L. Wang, C. Y. Ding, Z. W. Zhang, J. Liu, H. J. Yu and Y. P. Li, *Adv. Funct. Mater.*, 2017, **27**, 1703674.

[15] S. M. Mahalingam, J. D. Ordaz and P. S. Low, *ACS Omega*, 2018, **3**, 6066-6074.

[16] J. S. Xu, F. Zeng, H. Wu, C. M. Yu and S. Z. Wu, *ACS Appl. Mater. Interfaces*., 2015, **7**, 9287-9296.

[17] D. Y. Cho, H. Cho, K. Kwon, M. J. Yu, E. Lee, K. M. Huh, D. H. Lee and H. C. Kang, *Adv. Funct. Mater*., 2015, **25**, 5479-5491.

[18] X. Wang, S. Peralta and C. T. Moraes, *Adv. Cancer. Res*., 2013, **119**, 127-160.

[19] Z. Y. Hou, Y. X. Zhang, K. Deng Y. Y. Chen, X. J. Li, X. R. Deng, Z. Y. Cheng, H. Z. Lian, C. X. Li and J. Lin, *ACS nano*, 2015, **9**, 2584-2599.

[20] Y. Hua, Z. H. Shao, A. Q. Zhai, L. J. Zhang, Z. Y. Wang, G. Zhao, F. W. Xie, J. Q. Liu, X. L. Zhao, X. Y. Chen and S. Q. Zang, *ACS nano*, 2023, https://doi.org/10.1021/acsnano.3c01068.

[21] K. Brodowska, A. Al-Moujahed, A. Marmalidou, M. M. Horste, J. Cichy, J. W. Miller, E. Gragoudas and D. G. Vavvas, *Exp. Eye. Res*., 2014, **124**, 67-73.

[22] J. Zielonka, J. Joseph, A. Sikora, M. Hardy, O. Ouari, J. Vasquez-Vivar, G. Cheng, M. Lopez and B. Kalyanaraman, *Chem. Rev*., 2017, **117**, 10043-10120.

[23] K. Nakamura, K. Yamashita, Y. Itoh, K. Yoshino, S. Nozawa and H. Kasukawa, *BBA-Biomembranes*, 2012, **1818**, 2801-2807.

[24] A. A. Zaki, D. Joh, Z. L. Cheng, A. L. B. D. Barros, G. Kao, J. Dorsey and A. Tsourkas, *ACS Nano*, 2014, **8**, 104-112.

[25] S. Ip, C. M. MacLaughlin, N. Gunari and G. C. Walker, *Langmuir*, 2011, **27**, 7024-7033.

[26] A. J. Mieszawska, W. J. M. Mulder, Z. A. Fayad and D. P. Cormode, *Mol. Pharmaceutics*, 2013, **10**, 831-847.

[27] Q. Y. Bao, A. Y. Liu, Y. Ma, H. Chen, J. Hong, W. B. Shen, C. Zhang and Y. Ding, *Colloid. Surface. B.*, 2016, **146**, 475-481.

[28] G. V. Orsinger, J. D. Williams and M. Romanowski, *ACS Nano*, 2014, **8**, 6151-6162.

[29] R. Vankayala, Y. K. Huang, P. Kalluru, C. S. Chiang and K. C. Hwang, *Small*, 2014, **10**, 1612-1622.

[30] S. J. Wang, J. Xin, L. W. Zhang, Y. C. Zhou, C. P. Yao, B. Wang, J. Wang and Z. X. Zhang, *Int. J. Nanomed*., 2018, **13**, 2143-2160.

[31] G. V. White, Y. J. Chen, J. Roder-Hanna, G. D. Bothun and C. L. Kitchens, *ACS Nano*, 2012, **6**, 4678-4685.

[32] Z. Kautzka, S. Clement, E. M. Goldys and W. Deng, *Int. J. Nanomed*., 2017, **12**, 969-977.

[33] E. Y. Chuang, C. C. Lin, K. J. Chen, D. H. Wan, K. J Lin, Y. C. Ho, P. Y. Lin and H. W. Sung, *Biomaterials*, 2016, **93**, 48-59.

[34] C Fenzl, T Hirsch and A. J. Baeumner, *Anal. Chem*., 2015, **87**, 11157-11163.

[35] X. F. Gu, C. Shen, H. Li, E. M. Goldys and W. Deng, *J. Nanobiotechnol*., 2020, **18**, 87.

[36] P. Liang, L. S. Mao, Y. L. Dong, Z. W. Zhao, Q. Sun, M. Mazhar, Y. N. Ma, S. J. Yang and W. Ren, *Pharmaceutics*. 2021, **13**, 2070.

[37] D. R. Cooper, D. Bekah and J. L. Nadeau, *Front. Chem*., 2014, **2**, 86.

[38] B. Fateye, A. Wan, X. Yang, K. Myers and B. Chen, *Photodiagn. Photodyn*., 2015, **12**, 19-26.

[39] J. P. Celli, N. Solban, A. Liang, S. P. Pereira and T. Hasan, *Laser. Surg. Med*., 2011, **43**, 565-574.

[40] S. Kwon, Y. Lee, Y Jung, J. H. Kim, B. Baek, B. Lim, J. Lee, I. Kim and J. Lee, *Eur. J. Med. Chem*., 2018, **148**, 116-127.

[41] C. X. Wang and R. J. Youle, *Annu. Rev. Genet*., 2009, **43**, 95-118.

[42] I. Noh, D. Y. Lee, H. Kim, C.-U. Jeong, Y. Lee, J.-O. Ahn, H. Hyun, J.-H. Park and Y.-C. Kim, *Adv. Sci*., 2018, **5**, 1700481.

[43] Y. N. Tan, Y. Zhu, Y. Zhao, L. J. Wen, T. T. Meng, X. Liu, X. Q. Yang, S. H. Dai, H. Yuan and F. Q. Hu, *Biomaterials*, 2018, **154**, 169-181.

[44] S. A Lakhani, A. Masud, K. Kuida, G. A. P. Jr, C. J. Booth, W. Z. Mehal, I. Inayat and R. A. Flavell, *Science*, 2006, **311**, 847-851.

[45] A. G. Anwer, M. E. Gosnell, S. M. Perinchery, D. W. Inglis and E. M. Goldys, Perinchery, *Laser. Surg. Med*., 2012, **44**, 769-778.

[46] F. Ahmad, X. Y. Wang, Z. Jiang, X. J. Yu, X. Y. Liu, R. H Mao, X. Y. Chen, W. W Li, *ACS Nano*, 2019, **13**, 10419-10433.